Gating Properties of Gap Junction Channels Assembled from Connexin43 and Connexin43 Fused with Green Fluorescent Protein

Feliksas F. Bukauskas, Angele Bukauskiene, Michael V. L. Bennett, and Vytas K. Verselis
Department of Neuroscience, Albert Einstein College of Medicine, Bronx, New York 10461 USA

ABSTRACT We used cell lines expressing wild-type connexin43 (Cx43) and Cx43 fused with enhanced green fluorescent protein (Cx43-EGFP) to examine mechanisms of gap junction channel gating. Previously it was suggested that each hemichannel in a cell-cell channel possesses two gates, a fast gate that closes channels to a nonzero conductance or residual state via fast ($<\sim$2 ms) transitions and a slow gate that fully closes channels via slow transitions ($>\sim$10 ms). Here we demonstrate that transjunctional voltage (V_j) regulates both gates and that they are operating in series and in a contingent manner in which the state of one gate affects gating of the other. Cx43-EGFP channels lack fast V_j gating to a residual state but show slow V_j gating. Both Cx43 and Cx43-EGFP channels exhibit slow gating by chemical uncouplers such as CO_2 and alkanols. Chemical uncouplers do not induce obvious changes in Cx43-EGFP junctional plaques, indicating that uncoupling is not caused by dispersion or internalization of junctional plaques. Similarity of gating transitions during chemical gating and slow V_j gating suggests that both gating mechanisms share common structural elements. Cx43/Cx43-EGFP heterotypic channels showed asymmetrical V_j gating with fast transitions between open and residual states only when the Cx43 side was relatively negative. This result indicates that the fast V_j gate of Cx43 hemichannels closes for relative negativity at its cytoplasmic end.

INTRODUCTION

A property common to gap junction (GJ) channels formed of connexins and most innexins is sensitivity of junctional conductance, g_j, to transjunctional voltage, V_j, the voltage difference between cells (Verselis and Veenstra, 2000). In homotypic junctions, reductions in g_j with V_j are usually symmetric about a maximum at $V_j = 0$. A distinct feature of V_j gating is that steady-state g_j does not decline to zero with increasing V_j and may appear to reach a plateau at a residual value that varies from $\sim$5% to 30% of the maximum g_j depending on the connexin type. Single-channel studies show that residual g_j is due to incomplete closure of the GJ channel by the V_j; i.e., V_j causes channels to close to a subconductance state, often termed the residual state (Weingart and Bukauskas, 1993; Bukauskas and Weingart, 1994, Moreno et al., 1994). It is widely accepted that each hemichannel in a formed GJ channel has its own V_j gate and for each polarity of V_j, closure can be ascribed to one or the other hemichannel. Closure of hemichannels in GJ channels formed of connexins can be of either polarity, and the opposite gating polarities of two closely related connexins, Cx32 and Cx26, was shown to be reversed by changing the charge of a single amino acid residue at the second position of the N-terminus (NT) (Verselis et al., 1994; Oh et al., 2000).

GJ channels can also be gated by chemical factors such as alkanols, H^+, and Ca^{2+} (Bennett and Verselis, 1992). Treatment with heptanol or octanol or raising cytoplasmic H^+ or Ca^{2+} reduces g_j, but unlike applications of V_j, reduces g_j to zero. Examination of gating by these agents at the single-channel level shows that these treatments close the channel fully rather than incompletely as with V_j gating. Also, unlike V_j gating, where the time course of the transitions between states is rapid and not resolvable due to frequency limitations of patch clamp amplifiers, chemical agents induce gating transitions that appear slow, taking tens of milliseconds for channels to transit between fully open and fully closed states (Bukauskas and Weingart, 1994; Bukauskas and Peracchia, 1997). That V_j and chemical agents cause channels to gate to different levels via transitions with different kinetics suggests that two different types of gates mediate V_j and chemical gating.

Some hemichannels can function when unapposed, i.e., when they are not docked in a GJ channel configuration and show complex gating by voltage (Ebihara and Steiner, 1993; Trexler et al., 1996; Pfahnl and Dahl, 1998; Oh et al., 2000). Typically, closure at inside negative voltages is characterized by slow transitions to a fully closed state, reminiscent of chemical gating in GJ channels (Trexler et al., 1996; Pfahnl and Dahl, 1999; Oh et al., 2000). Hemichannel closures to substates via fast transitions, reminiscent of V_j gating, also occur at polarities that correspond to the polarities of V_j gating demonstrated in cell-cell channels (Trexler et al., 1996; Oh et al., 2000). Thus, unapposed hemichannels appear to contain two types of voltage gating mechanisms. Similarly, recordings of macroscopic junctional currents in pairs of *Xenopus* oocytes injected with Cx43 or Cx32 RNA were

Received for publication 23 January 2001 and in final form 28 March 2001.

Address reprint requests to Dr. Feliksas F. Bukauskas, Albert Einstein College of Medicine, Department of Neuroscience, 1300 Morris Park Avenue, Bronx, NY 10461. Tel.: 718-430-4130; Fax: 718-430-8944; E-mail: fbukausk@aecom.yu.edu.

0006-3495/01/07/137/16 $2.00

reported to have fast and slow components that were attributed to the action of two different V_j gating mechanisms in each hemichannel (Revilla et al., 1999). In addition, gating to substates and to fully closed states in cell-cell channels can occur with V; (Bukauskas et al., 1995a,b; Oh et. al, 1999; Ramanan et al., 1999; Banach and Weingart, 2000). Furthermore, some GJ channels have been shown to be sensitive to V_m, as well as V_j (Obaid et al., 1983; Verselis et al., 1991; Bukauskas et al., 1992; Barrio et al., 1997; Manthey et al., 1999). Thus, gating of GJ channels is complex and appears to be mediated by multiple gating mechanisms. It is unclear the extent to which the different types of gating observed in GJ channels share common structural elements.

Recently we showed that GJ channels formed of Cx43 with enhanced green fluorescent protein (EGFP) attached to its carboxy terminus (CT) gate only via slow gating transitions between fully open and closed states reminiscent of chemical gating; no gating transitions to the residual substate, as observed in Cx43 channels, could be detected (Bukauskas et al., 2000). Here we examined, in more detail, gating by V_j in Cx43 and Cx43-EGFP channels and chemical gating in Cx43-EGFP channels. We found that at macroscopic and single-channel levels V_j-induced gating in Cx43 channels consists of fast gating transitions between open and residual states and slow transitions between either open or residual and fully closed states. Our data show that these two types of transitions, fast and slow, are mediated by separate gates, termed fast and slow gates, respectively. We show that the fast and slow gates operate in series whereby activation of the slow gate depends on whether the fast gate is open or closed, perhaps simply because the voltage across the slow gate's voltage sensor is reduced by closure of the fast gate. Attachment of EGFP to the CT of Cx43 leaves only the slow gate operational. Heterotypic Cx43/Cx43-EGFP channels show that the fast gate closes for only one polarity of V_j, consistent with the disruption of this gate by EGFP being confined to the Cx43-EGFP hemichannel. The asymmetry in gating at macroscopic and single-channel levels indicates that the fast gate closes when Cx43 hemichannels are made relatively negative at their cytoplasmic ends. In addition, monitoring the fluorescence of Cx43-EGFP junctional plaques with application of heptanol and CO_2, which induced complete uncoupling, showed no obvious change in plaque integrity even when applications were prolonged and uncoupling rendered poorly reversible. These data suggest that chemical uncoupling agents do not cause gross dispersion of the GJ channel plaques. Preservation of chemical gating and V_j gating to fully closed states in Cx43-EGFP channels, together with the similarity in their gating transitions, suggests that they share common structural elements.

MATERIALS AND METHODS

cDNAs, cell lines, culture conditions, and transfections

The cDNA encoding Cx43-EGFP was constructed as described by Jordan et al. (1999). Experiments were performed on HeLa cells (a human cervix carcinoma cell line, ATCC CCL-2) stably transfected with cDNAs encoding rat Cx43 and rat Cx43-EGFP and on Novikoff cells (a rat hepatoma cell line) that endogenously express Cx43 (Meyer et al., 1991). HeLa cells were grown in Dulbecco's medium supplemented with 10% fetal bovine serum. All media, sera, and culture reagents were obtained from Life Technologies (GIBCO BRL, Gaithersburg, MD). Transfections were performed on HeLa cells grown to 50–75% confluency in 35 culture dishes in Opti-MEM1 medium containing LipofectAMINE (GIBCO BRL) and 1 μg of plasmid DNA. For selection of stable transfectants, cells were trypsinized and plated at dilutions of ~1:20 in the presence of 0.3–1.0 mg/ml G418 (GIBCO BRL). The selection media was changed every 3 days for 2–3 weeks. Individual colonies were selected with cloning cylinders, trypsinized, and expanded into clonal cell lines. Stably transfected cells were screened for Cx43-EGFP expression by fluorescence microscopy. To study homotypic junctions, cells of one type were seeded at a density of $\sim 10^4$ cells/cm^2 onto sterile coverslips placed in multi-well culture dishes. To study Cx43/Cx43-EGFP heterotypic junctions, HeLaCx43 or Novikoff and HeLaCx43-EGFP cells were mixed together in equal quantities and seeded on coverslips at $\sim 10^4$ cells/cm^2. Novikoff cells were grown in Swim's S-77 medium with 4 mM glutamine, 20% horse serum, and 5% fetal bovine serum. Three weeks before co-culturing with HeLa cells, they were transferred to Dulbecco's medium.

Electrophysiological measurements

For simultaneous electrophysiological and fluorescence recording, cells were grown on 22 × 22-mm number 0 coverslips and transferred to an experimental chamber mounted on the stage of an inverted microscope equipped with phase-contrast optics and a fluorescence imaging system. The chamber was perfused with a modified Krebs-Ringer solution containing (in mM): 140 NaCl, 4 KCl, 2 $CaCl_2$, 1 $MgCl_2$, 5 HEPES, 5 glucose, 2 pyruvate (pH 7.4). Patch pipettes were filled with a solution containing (in mM): 10 NaCl, 140 KCl, 0.2 $CaCl_2$, 1 $MgCl_2$, 3 MgATP, 5 HEPES (pH 7.2), 2 EGTA ($[Ca^{2+}]_i = 5 \times 10^{-8}$ M). Junctional conductance was measured using the dual whole-cell patch clamp (Neyton and Trautmann, 1985; White et al., 1985). Briefly, each cell of a pair is voltage clamped independently with a separate patch clamp. By stepping the voltage in one cell and keeping the other constant, junctional current, I_j, is observed directly as a change in current in the unstepped cell. Thus, for stepping cell 1, g_j is obtained by dividing the change in I_2 by the change in V_1. With low levels of coupling, unitary junctional currents are recorded as discrete quantal changes in the unstepped cell that are accompanied by equal and opposite quantal changes in the stepped cell. Voltages and currents were recorded on videotape using a data recorder, VR-100 (Instrutech Corp., Port Washington, NY), and were subsequently digitized using a MIO-16X A/D converter (National Instruments, Austin, TX) using our own acquisition software. Records were digitized at 5 kHz and filtered at 1 kHz.

Cx43-EGFP fluorescence measurements

Fluorescence signals were monitored using an Olympus IX70 inverted microscope (Olympus America, Melville, NY) equipped with an imaging system containing an OlymPix 2000 cooled digital camera (12 bit), a SpectraMASTER high-speed monochromator and UltraVIEW software for image acquisition and analysis (Perkin-Elmer Life Sciences, Boston, MA). Light delivery was accomplished with a liquid light guide. The wavelength used for excitation of EGFP was 480 nm. For emission, we used a 520 ±

20-nm filter and 495-nm beam splitter (Chroma Technology Corp., Brattleboro, VT). Electronic shuttering of the digital camera allowed setting exposure times and timing intervals between fluorescence measurements.

RESULTS

The conductance of Cx43 channels shows complex V_j dependence in macroscopic studies

Application of V_j steps to one cell of a coupled pair decreased G_j, the value of g_j normalized to the maximum value, g_{max}, at $V_j = 0$. G_j declined substantially between ± 30 mV and ± 80 mV to a value close to the residual G_j previously reported for this connexin (Perez-Armendariz et al., 1994; Valiunas et al., 1997). Fig. 1 *A* shows G_j measured at the ends of 30-s V_j steps over a ± 140-mV range. Data were pooled from HeLa cells transfected with Cx43, HeLaCx43 (filled circles), and Novikoff cells (open circles), which endogenously express Cx43. The solid line in Fig. 1 *A* is a fit of the data to a Boltzmann relation: $G_j = (1 - G_{min})/(1 + \exp(A \times (V_j - V_o))) + G_{min}$, where G_{min} is the normalized residual g_j, A is a measure of voltage sensitivity in mV^{-1} and V_0 is the V_j at which G_j is halfway between the maximum and minimum values. The best fit indicated a G_{min} of ~0.2 for either polarity of V_j, but the fit was poor at V_j values exceeding ± 100 mV with G_j seemingly approaching zero at sufficiently large V_j values. Data from Novikoff cells superimpose with that from HeLaCx43, indicating that the complex V_j gating we observed is likely intrinsic to Cx43 and not cell dependent or the result of contamination by endogenous connexins. All cell pairs were tested for the presence of cytoplasmic bridges by applying uncoupling agents such as heptanol and CO_2. Approximately 10% of 52 electrically coupled cell pairs examined in this study were excluded due to lack of full uncoupling by these chemical agents.

The kinetics underlying the changes in G_j were complex. Fig. 1, *B–D*, shows records of junctional currents, I_j values, from HeLaCx43 cell pairs in response to V_j steps of -52 mV, -90 mV, and -125 mV. In between the V_j steps, small, brief V_j test pulses were applied to evaluate recovery of g_j. Above each record of I_j, the calculated g_j is also plotted. At a $V_j = -52$ mV, g_j declined slowly reaching ~50% of its control value after 30 s (Fig. 1 *B*). The conductance did not reach steady state within the 30-s V_j step, which was characteristic at this and smaller V_j values (data not shown). Upon termination of the V_j step, two components of recovery were evident, a fast component that restored ~60% of the decline in g_j within the first test pulse followed by a slow recovery that took tens of seconds to fully restore g_j. At a larger V_j of -90 mV, the decline in g_j was faster and larger and appeared to reach a steady state ~1/3 of the maximum g_j (Fig. 1 *C*). Also, the g_j recovered rapidly, being fully restored within the first test pulse following termination of the V_j step. At a V_j of -125 mV, g_j declined more rapidly and again reached a value ~1/3 of the maximum g_j and then continued to decline slowly for the duration of the V_j step (Fig. 1 *D*). A slow decline following a rapid decline was very evident, with V_j values exceeding ± 100 mV, and was more prominent with increasing V_j values. The slow component of the decline at large V_j values gave rise to decline in G_j beyond calculated value of G_{min}. Upon termination of the -140-mV V_j step, two components of recovery were again evident, a rapid component that restored ~60% of g_j followed by a slow component that took tens of seconds.

Cx43 expressed in mammalian cells shows no evidence of V_m dependence

Recently it has been reported that junctions formed of wild-type and mutants of Cx43 in *Xenopus* oocyte pairs are sensitive to transmembrane or inside-out voltage, V_m, as well as V_j (Revilla et al., 2000). We tested for V_m dependence in HeLaCx43 and HeLaCx43-EGFP cell pairs by monitoring I_j with small repeated test pulses applied to one cell while equally and simultaneously changing the membrane potentials of both cells (Fig. 2 *A*). In the example shown, changes in V_m of 70 and 85 mV did not cause any noticeable change in the magnitude of I_j in response to the test pulses in the HeLaCx43 cell pair. A plot of normalized G_j (normalization to g_j value at $V_m = -50$ mV) as a function of V_m shows no significant dependence of G_j on V_m either in HeLaCx43 (open circles; four experiments) or in HeLaCx43-EGFP (open squares; five experiments) cell pairs; solid line is a data fit to a linear relation of the first order (Fig. 2 *B*).

Voltage gating of Cx43 GJ channels at the single-channel level: two types of gating transitions

Voltage gating of Cx43 at the single-channel level was examined in poorly coupled cell pairs (Fig. 3). In the example shown in Fig. 3 *B*, a V_j step of 37 mV showed four channels open at the beginning of the V_j step and two closing transitions ~110 pS in magnitude (see arrows) that were not reversed before the termination of the V_j step. Also evident were several brief transitions, ~85 pS in magnitude (see stars). Based on our previous studies of single Cx43 channels (Bukauskas and Peracchia, 1997; Bukauskas et al., 2000), the 110-pS steps correspond to transitions between open (γ_{open}) and fully closed (γ_{closed}) states and the 85-pS steps to transitions between γ_{open} and the residual conductance state (γ_{res}). In this example, the full closings were predominantly responsible for the reduced current at the end of the V_j step; closings to γ_{res} did not contribute significantly to the decrease in I_j over time. An expanded time scale of the segment of this record (inset) shows the 110-pS transitions to be slow (arrow), taking several milliseconds to fully close the channel. Larger V_j values typically caused I_j

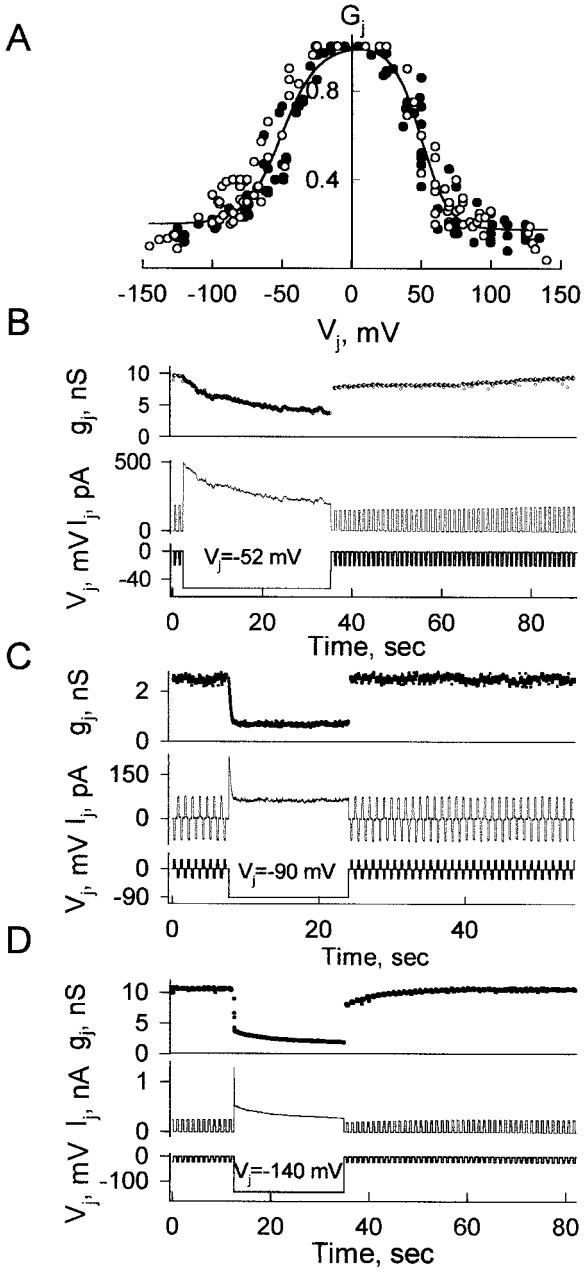

FIGURE 1 Voltage gating in HeLaCx43 and Novikoff cell pairs. (*A*) Pooled data of normalized g_j (G_j) versus V_j measured in Novikoff (○) and HeLaCx43 (●) cell pairs. G_j was measured at the ends of V_j steps from an initial common holding potential. The solid line is a fit of all the points to a Boltzmann relation. For larger V_j, g_j was reduced below the Boltzmann curve. The following Boltzmann parameters were obtained: $V_0 = 51 \pm 3$ mV, $A = 0.08 \pm 0.02$ mV^{-1} and $G_{min} = 0.2 \pm 0.03$ for negative V_j values and $V_0 = 50 \pm 2$ mV, $A = 0.09 \pm 0.02$ mV^{-1} and $G_{min} = 0.18 \pm 0.03$ for positive V_j values. (*B–D*) Examples of I_j records at V_j steps of 52 mV (*A*), 90 mV (*C*), and 140 mV (*D*). Repeated, small-amplitude V_j pulses, 200 ms in duration, were applied at 1-s intervals before and after the long-duration V_j steps to measure I_j recovery. The g_j-time dependencies determined from I_j and V_j records show kinetics of g_j decay and recovery. Application of a 52-mV V_j step (*B*) caused slow g_j decay. Recovery of g_j had fast and slow components. With a 90-mV V_j step (*C*), g_j decreased rapidly to a steady state and recovery was fast. With a 140-mV V_j step (*D*) at the beginning, g_j decreased rapidly and was followed by a slow decline in g_j that did not reach steady state during the duration of the step. The g_j recovery also showed two kinetic components, a fast component followed by a slow one.

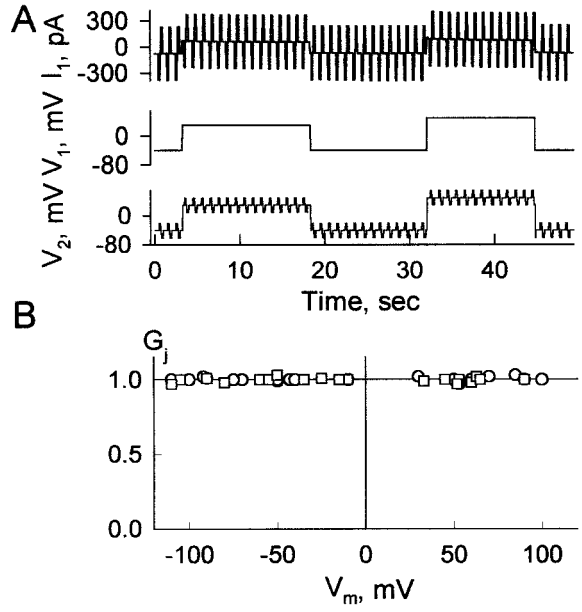

FIGURE 2 The g_j dependence on transmembrane or inside-out potential, V_m, in HeLaCx43 and HeLaCx43-EGFP cell pairs. (*A*) Illustrates that depolarization of both cells of the HeLaCx43 cell pair from the holding potential, −40 mV, to +40 and +50 mV did not cause any noticeable change in the magnitude of I_j in response to repeated test pulses of ±20 mV. V_1 and V_2 are the voltages in cell 1 and cell 2, respectively. (*B*) Pooled data of normalized g_j (G_j) versus V_m measured in HeLaCx43 (○; $n = 4$) and HeLaCx43-EGFP (□; $n = 5$) cell pairs; the regression line shows no effect of V_m on G_j.

to decline more rapidly, in agreement with the macroscopic data. However, as shown for a 69-mV V_j step (Fig. 3 *C*), the decrease in I_j occurred predominantly through stepwise transitions of 85 pS. In the record shown, one channel underwent a full 110-pS closing transition (arrow) and it remained closed for the duration of the V_j step. Also evident was a small 25-pS transition ascribable to full closure of a channel residing in γ_{res} (see inset and arrows). A slightly larger V_j of 75 mV (Fig. 3 *D*), similarly caused I_j to decline rapidly with stepwise transitions of 85 pS to reach a current corresponding to the residual value expected with all Cx43 channels residing in γ_{res}. Transitions to γ_{closed}, either from γ_{open} or γ_{res}, did occur but were rare and were not evident in this example. At larger V_j values, e.g., 107 mV (Fig. 3 *E*), I_j declined very rapidly (not resolvable with the time scale shown) to a level that corresponds to all channels residing in γ_{res}, but was followed by a slow decline in I_j through stepwise 25-pS transitions corresponding to full channel closures from γ_{res} (see histogram in inset). When examined at an expanded time scale (inset), the 25-pS transitions were

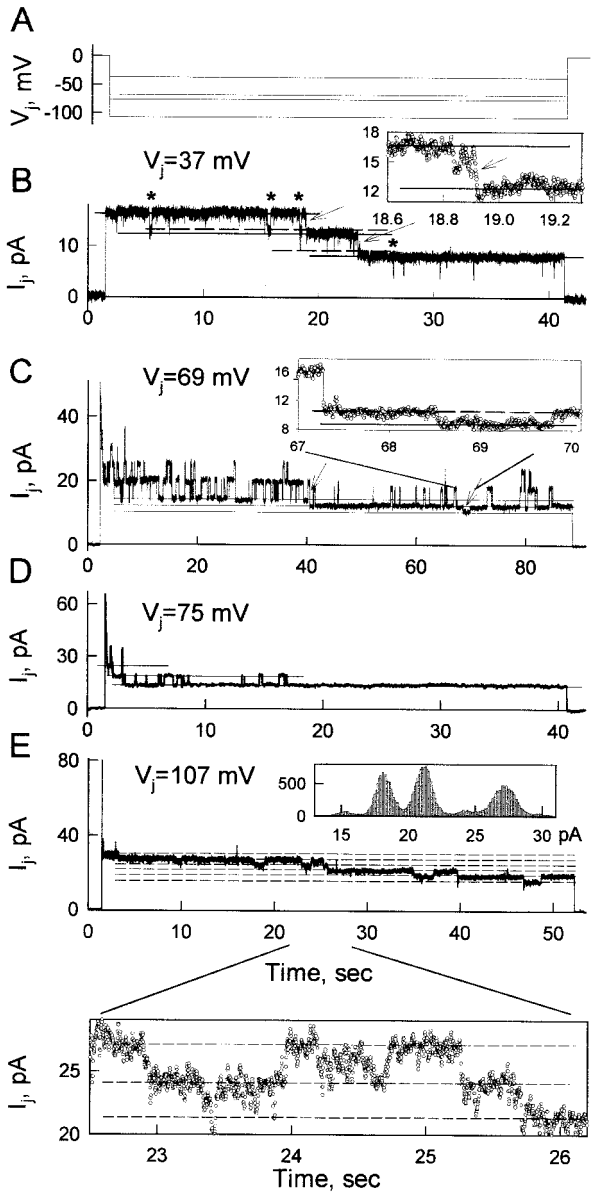

FIGURE 3 The g_j-V_j dependence of Cx43 at the single-channel level. (*A*) V_j steps applied to individual cell pairs. (*B*--*E*) I_j responses to V_j steps of 37 mV (*B*), 69 mV (*C*), 75 mV (*D*), and 105 mV (*E*). A V_j step of 37 mV (*B*) showed four channels open at the beginning of the V_j step and two closing transitions ~110 pS in magnitude (see *arrows*) that correspond to transitions between open and fully closed states. Also evident were several brief transitions, ~85 pS in magnitude (see *asterisks*). An expanded time scale (*inset*; sampling interval, 1 ms) shows that the 110-pS transitions are slow, taking several milliseconds to fully close the channel. At V_j = 69 mV (*C*), I_j declined rapidly through stepwise transitions of 85 pS. One channel underwent full 110-pS closing transition (*first arrow*). Also evident was a small 25-pS slow transition ascribable to full closure of a channel residing in γ_{res} (*second* arow; also see *inset*; sampling interval, 5 ms). At V_j = 75 mV (*D*) all the channels rapidly closed to the residual state with stepwise transitions of 85 pS. At V_j = 107 mV (*E*), I_j declined very rapidly to a level that corresponds to all channels residing in γ_{res} and was followed by a slow decline in I_j through stepwise 25-pS transitions corresponding to full channel closures from γ_{res} (see histogram in *inset*). The expanded time scale (*inset*; sampling interval, 2 ms) shows the 25-pS transitions to be slow, taking several milliseconds to complete.

slow, taking several milliseconds to complete. A decline in I_j via the 25-pS transitions continued with V_j steps as long as 2–3 min (data not shown).

Fig. 4 illustrates single-channel *I-V* curves obtained by applying voltage ramps from −100 mV to +100 mV to a cell pair recovering from uncoupling with 100% CO_2. A single-channel conductance, γ, plot over time was determined from I_j and V_j records as I_j/V_j. Open-channel current is essentially linear with voltage (solid line) yielding a slope conductance of ~110 pS (see corresponding solid line on the γ versus time plot). In these ramps, gating transitions were evident predominantly between γ_{open} and γ_{res}; transitions to γ_{closed} were rare, consistent with the slow kinetics of this process. A dashed line drawn through the current levels ascribed to γ_{res} corresponds to a slope conductance of ~25 pS (dashed line). Cx43 channels expressed in Novikoff and in HeLa cells behaved in the same way.

These single-channel data demonstrate that V_j elicits two types of gating in Cx43 channels. One type of gating is characterized by transitions between γ_{open} and γ_{res} and the other by transitions to γ_{closed} either from γ_{open} or γ_{res}. The latter gating has slow kinetics and can explain the slow component of the decline and recovery of g_j that we observe macroscopically. Gating between γ_{open} and γ_{res} has faster kinetics and can explain the faster component of decay and recovery of g_j that we observe macroscopically. Increasing V_j leads to faster reductions in g_j mediated increasingly by gating transitions between γ_{open} and γ_{res} giving rise to fast

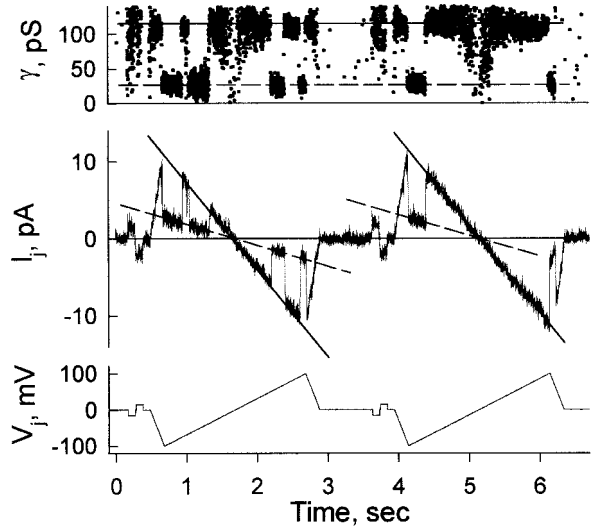

FIGURE 4 I_j-V_j relationship of a single Cx43 channel. Data shown are from a HeLaCx43 cell pair. The voltage protocol applied to one cell consisted of brief (100 ms) ± 15-mV V_j steps preceding V_j ramps from −100 to +100 mV, 2 s in duration (*bottom trace*). The junctional current record (*middle trace*) shows a linear I_j-V_j relationship in the open state (——) and the residual state of the component hemichannels (— — —). The conductance calculated every millisecond (*upper trace*) shows open and residual conductances: γ_{open} = 110 pS and γ_{res} = 25 pS.

recovery. High V_j values exceeding ±100 mV invoke gating to γ_{closed} from γ_{res} giving recovery with both fast and slow components.

V_j dependence of Cx43-EGFP channels; gating to the residual substate is lost

Unlike Cx43 channels, Cx43-EGFP channels exhibit only slow transitions between γ_{open} and γ_{closed}. When examined macroscopically, the reductions in g_j were always slow, as was recovery, and Cx43-EGFP junctions demonstrated less sensitivity to V_j gating than wild-type Cx43 junctions (Bukauskas et al., 2000). The data were collected in HelaCx43-EGFP cell pairs with g_j values between 7 and 20 nS. Because these g_j values can lead to underestimation of the dependence of g_j on V_j due to series resistance (Wilders and Jongsma, 1992), we repeated these measurements on poorly coupled HeLaCx43-EGFP call pairs ($g_j < 5$ nS; $n = 7$). A G_j-V_j plot for one polarity of V_j shown in Fig. 5 *A* demonstrates that the sensitivity of Cx43-EGFP channels to V_j is weaker than for Cx43 junctions, declining gradually over the 100-mV V_j shown. No evidence of a plateau was apparent as G_j continued to decline with increasing V_j values, approaching zero. A fit to a Boltzmann relation resulted in a $G_{min} = 0.01 \pm 0.06$ and a substantially less steep and less sensitive relationship with V_j than Cx43 ($A = 0.09 \pm 0.02$ mV^{-1} and $V_0 = 50 \pm 2$ mV for Cx43 vs. $A = 0.05 \pm 0.01$ mV^{-1} and $V_0 = 66 \pm 3$ mV for Cx43-EGFP). An example of the slow time course of the decay in g_j with an applied V_j of −40 mV is illustrated in Fig. 5 *B*. A poorly coupled cell pair was chosen to illustrate that only one transition size of 110 pS was evident corresponding to full channel openings and closings. The infrequent number of opening and closing transitions over the course of ~100 s of recording is indicative of the slow kinetics.

V_j ramps and steps applied to cell pairs containing single active Cx43-EGFP channels confirm that unitary conductance of Cx43 is unaffected by the attachment of EGFP, that the I_j-V_j relationship for an open channel is linear (see solid line on I_j record in Fig. 5 *C*), and that gating occurs only between fully open and closed states (Fig. 5, *C* and *D*). The expanded time scale of the record shown in Fig. 5 *D* plots the current in 1-ms intervals (open circles) and demonstrates that all the transitions are slow, usually taking several milliseconds to complete.

Cx43 channels can be modeled with two series gates per hemichannel operating contingently

Our data suggest that Cx43 channels have two types of voltage gates, both sensitive to V_j, that differ in their kinetics and in the extent to which single-channel conductance is reduced upon closure. Plotted in Fig. 6 is the ratio of g_j measured using small (15–20 mV), brief (100–200 ms) test pulses applied just before (g_{jpre}) and after (g_{jpost}) a V_j step to individual cell pairs as illustrated in the recordings in Fig. 1, *B–D*. A g_{jpost}/g_{jpre} approaching unity indicates that recovery is rapid and complete by the time the first post-test pulse is applied and is characteristic of the rapid time course of recovery for the gating process involving transiting to the residual substate. A reduced g_{jpost}/g_{jpre} indicates the presence of a slow component of recovery. For Cx43-EGFP channels (Fig. 6 *A*), g_{jpost}/g_{jpre} decreases monotonically with V_j paralleling the V_j dependence of these channels; data were collected from six HeLaCx43-EGFP cell pairs. As previously shown, Cx43-EGFP channels possess slow kinetics of decay and recovery from V_j and show transitions only between open and fully closed states. For Cx43, g_{jpost}/g_{jpre} is similar to that for Cx43-EGFP at a V_j of ~40 mV, but increases with increasing V_j values, peaking near unity at ~75–80 mV (Fig. 6 *B*). Data were pooled from seven HeLaCx43 (open circles) and five Novikoff (filled circles) cell pairs. As shown previously in Fig. 3, *D* and *E*, closures to the residual substate in this V_j range largely predominate, indicating that the increase in g_{jpost}/g_{jpre} reflects a change in gating from full closures to partial closures to the residual substate. With increases in V_j beyond ~80 mV, g_{jpost}/g_{jpre} gradually decreases again and is consistent with a reemergence of gating transitions to the fully closed state but now from a residual state (Fig. 3 *E*).

Disappearance and reemergence of slow gating to full closures with V_j can be explained by assuming there are two V_j gates in series in each hemichannel and that closure of one gate reduces the V_j sensed by the other gate, which in effect makes gating of one gate contingent on the state of the other gate.

Cx43/Cx43-EGFP heterotypic channels: fast V_j gating is a hemichannel property

Cx43/Cx43-EGFP heterotypic channels were examined by co-culturing HeLaCx43 or Novikoff cells with HeLaCx43-EGFP cells. We sought cell pairs in which only one cell displayed EGFP fluorescence and at least one fluorescent plaque was present at the junction between the cells. Fig. 7 *A* illustrates such a heterotypic cell pair assembled of a HelaCx43 and a HeLaCx43-EGFP cell. The bottom cell exhibits fluorescence associated with the plasma membrane as well as the cytoplasm whereas the top cell exhibits no detectable fluorescence. The arrow indicates a junctional plaque in the region of cell-cell contact. An asterisk designates a large vesicle containing Cx43-EGFP fluorescence. Junctional conductance between these two cells was 32 nS. Fig. 7 *B* illustrates a linear array of three cells, a Novikoff and two HeLaCx43-EGFP cells. The Novikoff cell exhibits no fluorescence, whereas the HeLaCx43-EGFP cells on the right exhibit fluorescence associated with the plasma membrane as well with the junctional plaques between Novikoff and HeLaCx43-EGFP cells as well as between the two

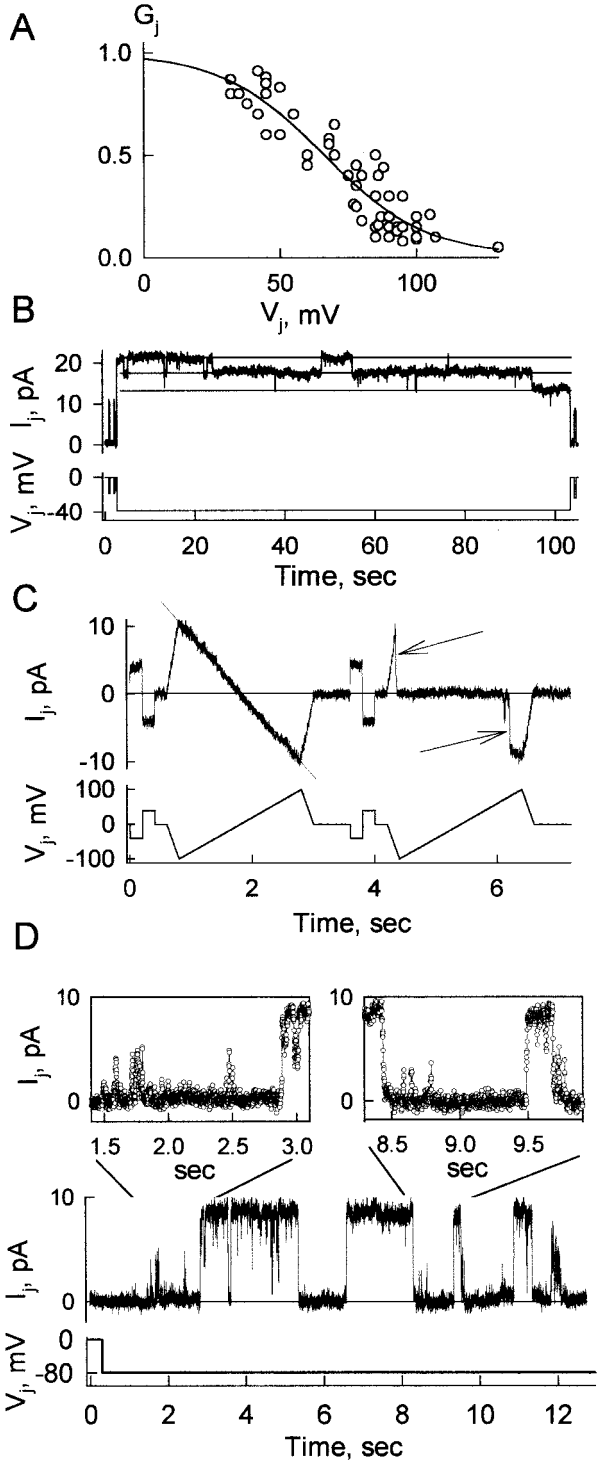

FIGURE 5 Voltage dependence of Cx43-EGFP GJs. (*A*) Pooled data of G_j-V_j dependence of Cx43-EGFP channels. Data are shown as open circles obtained from seven cell HeLaCx43-EGFP cell pairs. A fit to a Boltzmann relation resulted in a $V_0 = 66 \pm 3$ mV, $A = 0.05 \pm 0.01$ mV^{-1}, and $G_{min} = 0.01 \pm 0.06$ (——). (*B*) An example of I_j response to a V_j step of 40 mV in a HeLaCx43-EGFP cell pair with four functional channels. (*C*) Linear I_j-V_j relation at the single-channel level. The voltage protocol applied to one cell consisted of brief (200 ms) ± 40-mV V_j steps preceding V_j ramps from +100 to −100 mV, 2 s in duration. (*D*) Single GJ channel gating transitions at $V_j = 80$ mV in a cell pair measured during recovery from CO_2 application. Gating transitions were accompanied by multiple fluctuations that are illustrated in the two insets at an expanded time scale; interval between points is 1 ms.

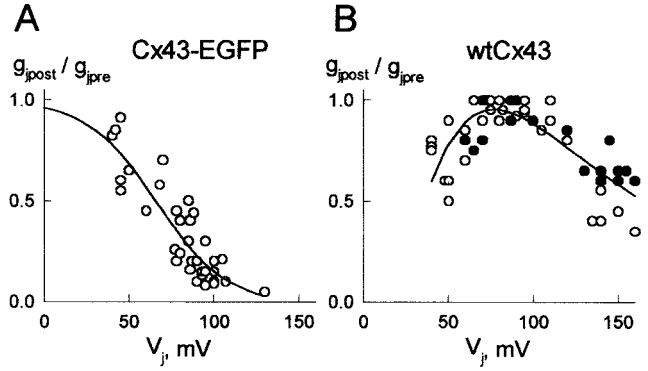

FIGURE 6 Recovery of g_j from V_j reveals interactions between fast and slow processes. Recovery of g_j was measured as a ratio g_{jpost}/g_{jpre}, where g_{jpre} and g_{jpost} are g_j values measured before and immediately following V_j steps ranging from +40 to +130 mV. (*A*) Plot of g_{jpost}/g_{jpre}-V_j obtained from HeLaCx43-EGFP cell pairs. g_{jpost}/g_{jpre} decreases as V_j increases, following the V_j dependence of g_j for Cx43-EGFP junctions. The solid line is a fit of the data to the Boltzmann relation with the following parameters: $V_0 = 66 \pm 6$ mV, $A = 0.05 \pm 0.01$ mV^{-1}, and $G_{min} = 0.02 \pm 0.11$. (*B*) Plot of g_{jpost}/g_{jpre}-V_j obtained from HeLaCx43 (○) and Novikoff (●) cell pairs. In contrast to Cx43-EGFP junctions, g_{jpost}/g_{jpre} shows a complex relationship with V_j. The solid line is a fit of the data to a peak function of the form, $g_{jpost}/g_{jpre} = a \times \exp(-0.5 \times (\ln(V_j/V_p)/b)^2)$, where V_p is the voltage at which g_{jpost}/g_{jpre} reaches a maximum and a and b are peak amplitude and steepness, respectively. Fit parameters are as follows: $V_p = 77 \pm 2$ mV, $a = 0.96 \pm 0.02$, and $b = 0.68 \pm 0.04$.

HeLaCx43-EGFP cells (arrows). Junctional conductance between the Novikoff and HeLaCx43-EGFP cells was 19 nS.

We recorded from 19 heterotypic cell pairs, with g_j ranging from 0.7 to 33 nS, and found V_j dependence to be highly asymmetric in each case. Gating resembled that of Cx43 channels with V_j values relatively negative on the Cx43 side. Conversely, gating resembled that of Cx43-EGFP channels with V_j values relatively negative on the Cx43-EGFP side. Shown in Fig. 8 is an example of junctional current in response to 30-s V_j steps of ±85 mV. Repeated, brief ±20-mV test pulses were applied before and after the long-duration V_j steps to monitor recovery. The time course of the decay in current was considerably faster upon hyperpolarizing the HeLaCx43 cell (relatively negative on the Cx43 side) than when depolarizing the same cell to the same extent (relatively negative on the Cx43-EGFP side). Also, I_j appeared to reach a steady-state residual level upon hyperpolarizing the HeLaCx43 cell but continued a slow decline toward zero for the opposite V_j polarity. Finally, recovery was much faster after hyperpolarizing the HeLaCx43 cell, being essentially complete within the first test pulse. Re-

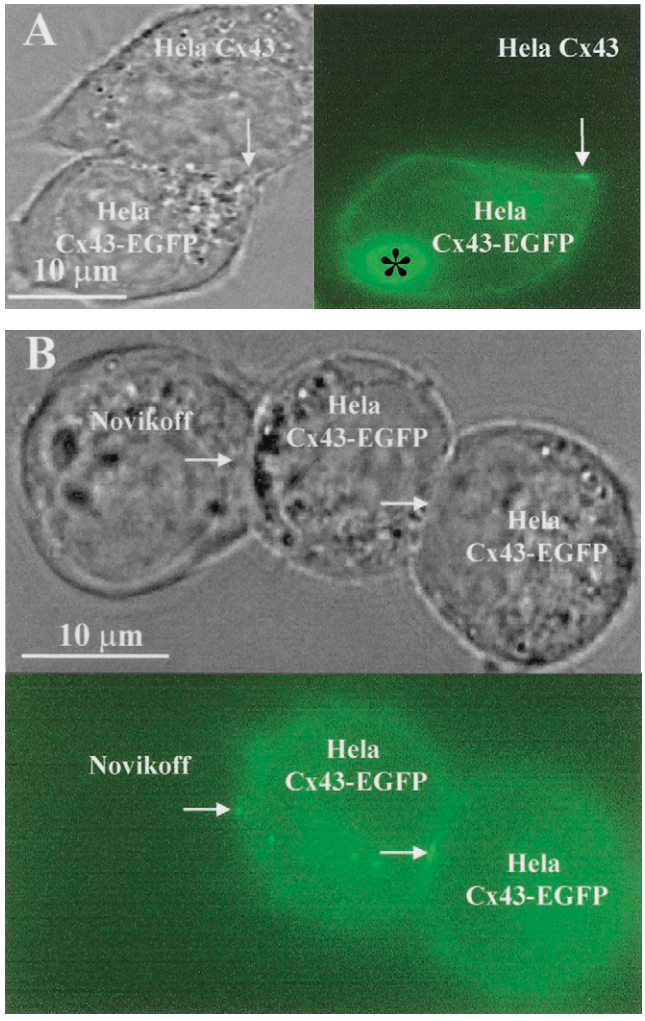

FIGURE 7 Illustration of junctional plaques formed between HeLaCx43, HeLaCx43-EGFP, and Novikoff cells. (*A*) Phase contrast (*left*) and fluorescent (*right*) images of a heterotypic HeLaCx43/HeLaCx43-EGFP cell pair. The junctional plaque is indicated by an arrow. Junctional conductance in this cell pair was 32 nS. The asterisk shows an internalized junctional plaque. (*B*) Phase contrast (*top*) and fluorescent (*bottom*) images of three cells, a HeLaCx43-EGFP cell contacted on one side by a Novikoff cell and on the other side by another HeLaCx43-EGFP cell. Junctional plaques formed between the Novikoff and the HeLaCx43-EGFP cells as well as between the HeLaCx43-EGFP cells. Junctional conductance measured between the Novikoff and the HeLaCx43-EGFP cells was 19 nS.

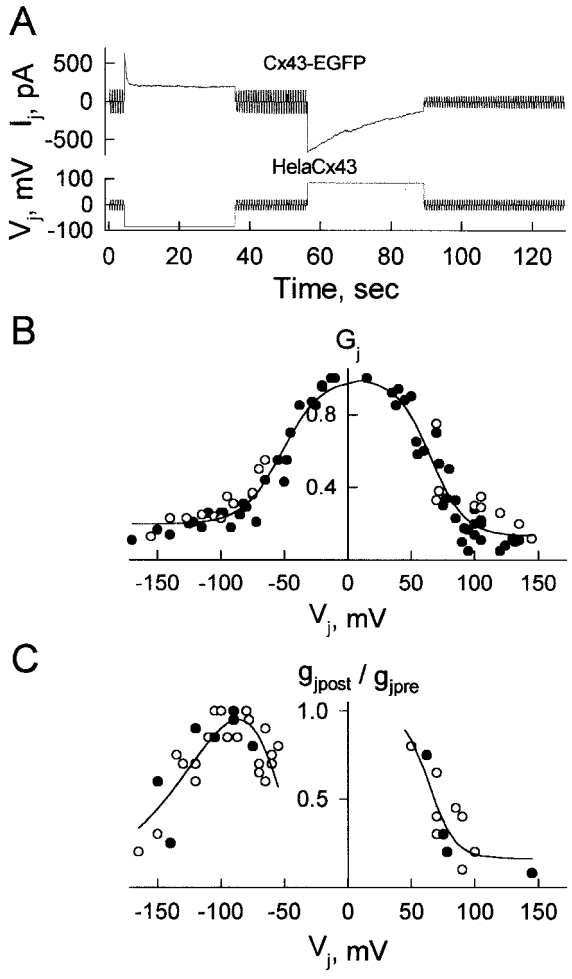

FIGURE 8 V_j dependence of Cx43/Cx43-EGFP heterotypic junctions. (*A*) Illustration of changes in I_j in response to ±85-mV steps applied to the HeLaCx43 cell. I_j decreased more slowly during the positive V_j step. Repeated ±25-mV pulses were applied between V_j steps to monitor the recovery of I_j. (*B*) g_j-V_j dependence of Cx43/Cx43-EGFP heterotypic junctions. Positive and negative V_j values indicate that the cell expressing Cx43 was made relatively positive and negative, respectively. The experimental data were taken from seven HeLaCx43/HeLaCx43-EGFP cell pairs (●) and from four Novikoff/HeLaCx43-EGFP (○) cell pairs. The solid lines for each polarity of V_j are fits of the data to the Boltzmann relation. The Boltzmann parameters are as follows: $V_0 = 51 \pm 4$ mV, $A = 0.07 \pm 0.01\text{mV}^{-1}$, and $G_{min} = 0.2 \pm 0.04$ for negative V_j values and $V_0 = 66 \pm 4$ mV, $A = 0.07 \pm 0.02$ mV^{-1}, and $G_{min} = 0.12 \pm 0.07$ for positive V_j values. (*C*) Dependence of g_{jpost}/g_{jpre} on V_j; positive and negative V_j values indicate that the cell expressing Cx43 was made relatively positive and negative, respectively. The experimental data were obtained from the same cell pairs shown in *B*. The solid line at negative V_j values is a fit of the data to the peak function described previously in Fig. 6. Parameters are as follows: $V_p = 86 \pm 2$ mV, $a = 0.95 \pm 0.04$, and $b = 0.45 \pm 0.04$. The solid line at positive V_j values is a fit of the data to the Boltzmann relation. Parameters are as follows: $V_0 = 64 \pm 4$ mV, $A = 0.09 \pm 0.04$ mV^{-1}, and $G_{min} = 0.16 \pm 0.1$.

covery from the other V_j polarity was slow, and in the example shown only ~50% of g_j recovered over the 40 s shown. Fig. 8 *B* summarizes data pooled from HeLaCx43/HeLaCx43-EGFP (*filled circles*) and Novikoff/HeLaCx43-EGFP (*open circles*) cell pairs. Plotted is G_j as a function of V_j. The decrease in G_j is asymmetric about $V_j = 0$ as previously indicated. We saw no difference when HeLaCx43-EGFP cells were paired to Novikoff cells or to HeLaCx43 cells.

Single Cx43/Cx43-EGFP channels were examined in poorly expressing cell pairs or during recovery from heptanol or CO_2 uncoupling. Fig. 9 *A* shows a record of I_j in a HeLaCx43/HeLaCx43-EGFP cell pair, when only a single channel was active. Application of a voltage protocol con-

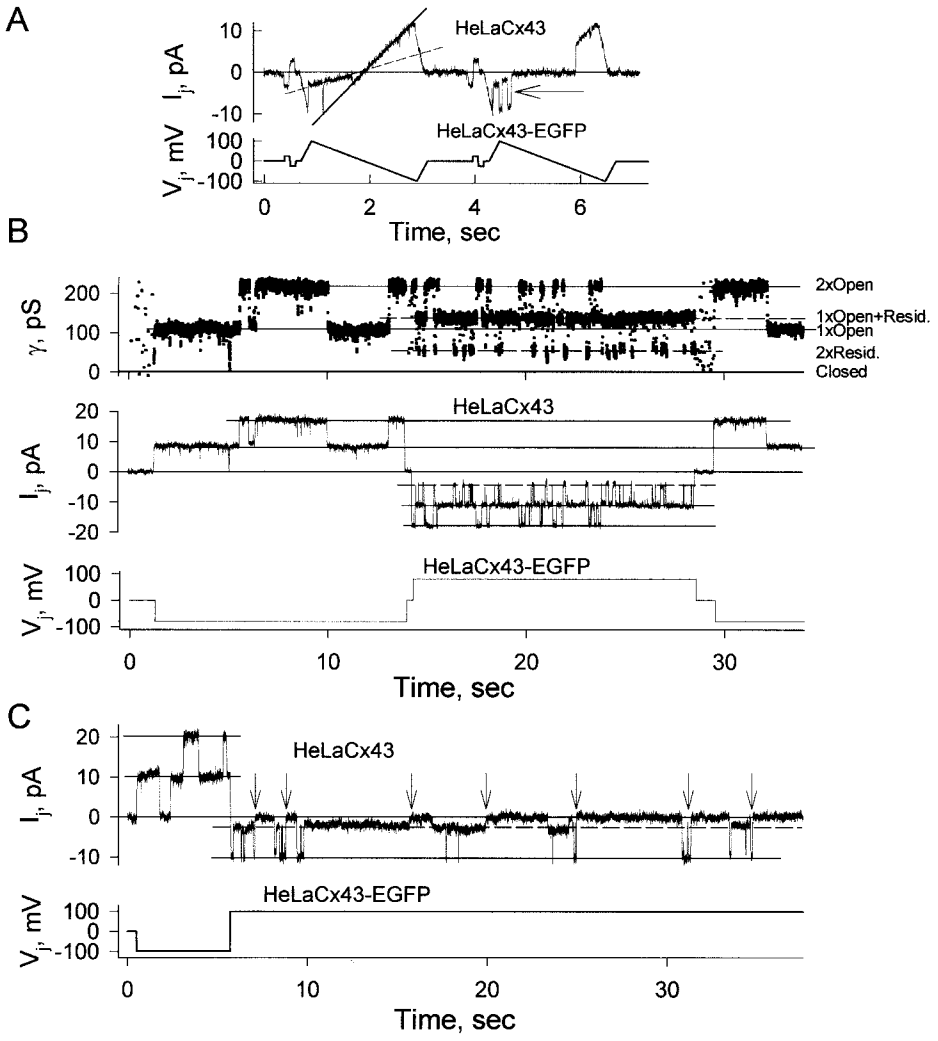

FIGURE 9 Illustration of asymmetric V_j gating in heterotypic Cx43/Cx43-EGFP junctions at the single-channel level. (*A*) I_j-V_j relationship of a single open channel in a HeLaCx43/HeLaCx43-EGFP cell pair measured in response to V_j ramps from −100 to +100 mV preceded by brief ±25-mV V_j steps and applied to the HeLaCx43-EGFP cell (*bottom trace*). The open channel current is essentially linear with V_j giving a slope conductance of ~110 pS (——). Gating transitions to the residual state (see *dashed line* during the first ramp) are evident only on the positive limb of the ramp. Infrequently, we observed gating transitions between open and fully closed states as indicated by the arrow in the second ramp. (*B*) Record of I_j during application of ±80-mV V_j steps. A voltage step of −80 mV applied to the HeLaCx43-EGFP cell shows gating transitions of ~110 pS between open and closed states. A +80-mV voltage step induces gating transitions of ~85 pS between open and residual state, predominantly (*dashed line* indicates the level of I_j with both channels in the residual state). A subsequent application of −80 mV again shows only gating transitions between open and fully closed states. (*C*) A large voltage step of −100 mV applied to the HeLaCx43-EGFP cell shows gating transitions of 110 pS between open and closed states much like that shown in *B* but with shorter open times. A voltage step of +100 mV shows three different types of gating transitions: ~85-pS transitions to the residual state (— — —), ~110-pS transitions to the fully closed state, and ~25-pS transitions between residual and closed state (all transitions to the closed state are indicated by *arrows*).

sisting of repeated ±20-mV, 200-ms V_j steps, followed by a 1-s, ±100-mV ramp applied to the HeLaCx43-EGFP cell shows a linear single-channel I_j-V_j relation for the open state (solid lines), giving a slope conductance of ~110 pS, indistinguishable from Cx43 or Cx43-EGFP homotypic channels. Typically, we observed gating transitions to the residual state only on the positive limb of the ramp (see dashed line during the first ramp negative on the Cx43 side). Infrequently, we observed gating transitions between open and fully closed states as indicated by the arrow in the second ramp. Fig. 9, *B* and *C*, shows records of I_j during applications of ±80-mV and ±100-mV V_j steps. A voltage step of −80 mV applied to the HeLaCx43-EGFP cell shows gating much like that for Cx43-EGFP channels; two channels were active and only full ~110-pS transitions were evident. Conversely, a +80-mV voltage step to the same cell shows gating much like that for Cx43 channels; transitions are more frequent and are predominantly ~85 pS in

magnitude. The dashed line indicates the level of I_j with both channels in the residual state. A subsequent application of the opposite V_j polarity again shows only gating transitions between open and fully closed states. A voltage step of −100 mV applied to the HeLaCx43-EGFP cell (see Fig. 9 *C*) shows gating much like that shown in Fig. 6 *B* at a V_j of −80 mV, but with shorter open times. A voltage step of +100 mV to the same cell shows rapid closure of channels with three different types of gating transitions: ~85-pS transitions to the residual state, ~110-pS transitions to the fully closed state, and ~25-pS transitions between residual (dashed line) and closed states; all transitions to the closed state are indicated by arrows.

Both macroscopic (Fig. 8) and single-channel (Fig. 9) data demonstrate that closure of the fast V_j gate to the residual state is a hemichannel property and occurs in the hemichannel that is made relatively negative on its cytoplasmic side.

Effects of chemical uncouplers on g_j and stability of Cx43-EGFP junctional plaques

A feature common to vertebrate GJ channels is closure in response to intracellular acidification and to a variety of applied chemicals, such as volatile anesthetics, alkanols, and arachidonic acid (Bennett and Verselis, 1992). It has been suggested that channel closure by volatile anesthetics and alkanols occurs by interaction with hydrophobic regions of connexins or with lipids, which may cause disruption of channel structure (Burt et al., 1991). As previously shown, coupling requires that plaques be present between cells at locations of cell-cell contact; cell pairs displaying only diffuse membrane staining do not show electrical coupling (Bukauskas et al., 2000). In HeLaCx43-EGFP cell pairs, we examined whether Cx43-EGFP channels retained sensitivity to chemical uncouplers and whether plaques were disrupted by these treatments. We tested heptanol, octanol, and CO_2 under conditions that cause full uncoupling of cells expressing Cx43. As for Cx43 channels, application of all those factors produced full uncoupling of Cx43-EGFP-expressing cells. Fig. 10 *B* shows a representative experiment demonstrating rapid uncoupling after heptanol application (3 mM) and coupling recovery during the washout period. Thus, attachment of EGFP to the CT of Cx43 does not interfere with the ability of either agent to cause channel closure. The lack of any observable effect on plaque integrity with heptanol is illustrated in Fig. 10 *A*. The cell pair shown had a single junctional plaque ~1.8 μm in diameter before heptanol application. Application of heptanol rapidly uncoupled this cell pair but had no observable effect on plaque size, shape, or fluorescence intensity. No observable effects were seen with applications of heptanol and octanol as long as 10 min even if recovery of g_j was incomplete.

Likewise, there was no identifiable effect on plaque integrity with application of 100% CO_2, except for a reduction in fluorescence intensity. Fig. 10 *C* shows a cluster of three cells with a single fluorescent plaque between two of them. The fluorescence image of the cells was taken after application of 100% CO_2. In this example, application of 100% CO_2 caused rapid uncoupling (see Fig. 10 *E*), but recovery of g_j was slow and incomplete. The junctional plaque, however, remained unchanged in size and shape (followed for 20 min). Shown in Fig. 10 *D* is the averaged Cx43-EGFP fluorescence intensity measured in two regions (squares 1 and 2), one containing the plaque and one containing diffuse Cx43-EGFP membrane staining; background fluorescence, measured in square 3, was subtracted. CO_2 reduced fluorescence of Cx43-EGFP to the same degree (~ 50%) and with the same time course whether it was aggregated in a plaque or distributed diffusely in the surface membrane.

Previously, we showed that attachment of EGFP to the CT of Cx43 abolished gating transitions between γ_{open} or γ_{res} (Bukauskas et al., 2000). We took advantage of the absence of fast V_j gating and the slow recovery of coupling with prolonged exposure to heptanol to examine single-channel events associated with chemical-induced gating (see Fig. 11). In this experiment, V_j was held at −45 mV at which there is infrequent voltage-induced gating allowing visualization of junctional current transitions induced by heptanol. Fig. 11 *A* shows a current record during washout from a 2-min heptanol application that was followed by a second heptanol application. Junctional current increased during washout in a stepwise fashion and declined very rapidly upon the reapplication of heptanol. The size of the individual transitions upon heptanol washout and reapplication are illustrated with amplitude histograms taken from the indicated segments. All transitions were found to be uniform and ~110 pS in amplitude corresponding to full channel closed/open transitions.

Fig. 11 *B* illustrates that the first opening transition took ~10 ms to complete and the last closing transition ~7 ms (intervals between points are 2.5 ms). Similar relatively slow gating transitions between open and closed states have been shown to characterize CO_2 gating in Cx43 channels (Bukauskas and Peracchia, 1997). To quantitate the time course of these transitions, we measured the mean time it took to go from 10% to 90% of a full transition. Under heptanol the mean closing and opening transition times were 7.8 ± 2.3 ms (n = 15) and 6.3 ± 2.1 ms (n = 12), respectively.

DISCUSSION

Two distinct V_j gating mechanisms in Cx43 gap junction channels

Studies of GJ channels in insect cells were the first to demonstrate that V_j closes GJ channels to γ_{res}, the residual conductance state, through fast gating transitions (Weingart

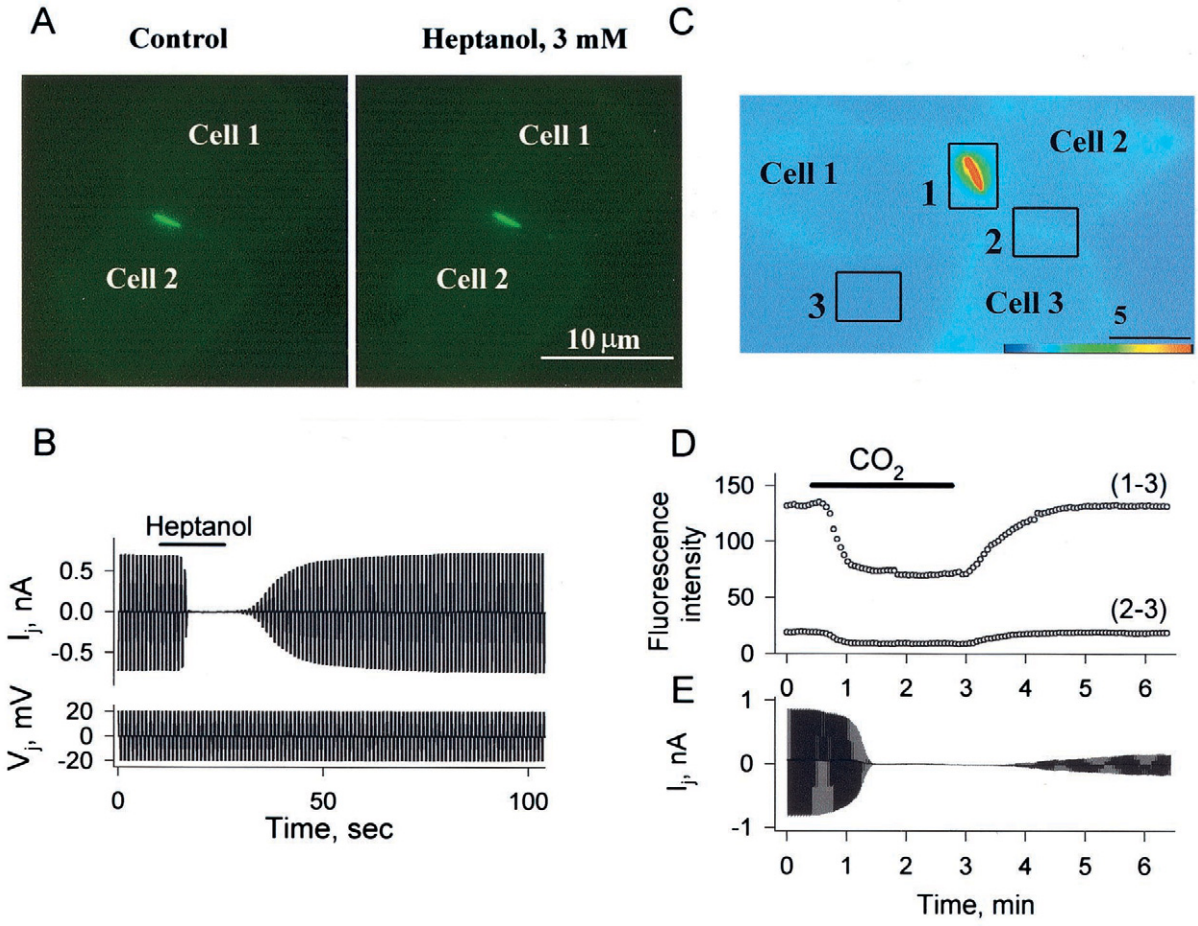

FIGURE 10 Effect of uncoupling agents on Cx43-EGFP fluorescence and g_j in HeLa cells. (*A*) Fluorescence images of a cell pair with a single large junctional plaque between the cells. The plaques were unchanged during application of 3 mM heptanol for 15 s. (*B*) Record of I_j in the cell pair shown in *A*. I_j was measured by applying brief (200-ms) V_j steps, ±20 mV alternating with a frequency of 1 Hz for each polarity. The bar denotes the duration of heptanol application. g_j decreased to zero and recovered fully. (*C*) Image of three cells showing a large plaque between two of them (labeled cell 1 and cell 2). Fluorescence intensity is shown in pseudo-color. Squares indicate regions from which mean fluorescence intensity was measured. Square 1 contains the plaque fluorescence and square 2 contains fluorescence diffusely distributed in the apposed membrane and cytoplasm. Square 3 is a region in which cells were absent and shows background fluorescence. (*D*) Effect of CO_2 on Cx43-EGFP fluorescence. Plots show fluorescence intensity taken from regions 1 and 2 with background fluorescence in region 3 subtracted. The bar denotes duration of 100% CO_2 application. Both signals decreased during CO_2 application but recovered fully. (*E*) Record of I_j between cells 1 and 2 shown in *C* during 100% CO_2 application. I_j was measured as in *B*.

and Bukauskas, 1993; Bukauskas and Weingart, 1994). Similar V_j-sensitive gating to γ_{res} has been demonstrated in vertebrate GJs both in cells transfected with connexin cDNAs (Moreno et al., 1994; Bukauskas et al., 1995a,b; Manthey et al., 1999) and cells expressing native connexins (Bukauskas and Peracchia, 1997; Valiunas et al., 1997). Although GJ channels have been shown to gate to multiple substates, γ_{res} is distinguished from the other substates by its long mean dwell time. Also, the value of γ_{res} relative to the open state γ_{open} largely accounts for the plateau of the steady-state conductance, G_{min}, observed macroscopically. However, for some connexins, e.g., Cx38 and Cx45, there is a discrepancy between the apparent macroscopic G_{min} and the ratio of γ_{res} to γ_{open} (Moreno et al., 1995), and as we demonstrate here for Cx43, G_{min} is not clearly expressed as g_j continues to decline gradually toward zero with increasing V_j values. Consistent with a decline in g_j toward zero, we show closing transitions induced by V_j are not always to substates, but also includes transitions to γ_{closed}.

Recently, it was reported in RIN cells transfected with Cx43 that V_j induces two types of gating transitions, fast transitions to γ_{res} and slow transitions to γ_{closed} (Banach and Weingart, 2000). These authors suggested that the fast and slow transitions to the residual and closed states, respectively, represent distinct gating mechanisms, with slow transitions comprising a less prominent mechanism evident at large V_j values. Although slow transitions could be detected at V_j values as small as ±40 mV, albeit infrequently, the frequency of occurrence did not increase until V_j exceeded ±80 mV. Our studies are in agreement that there are two types of gating transitions in Cx43 induced by V_j, but we also demonstrate a complex interaction between the two

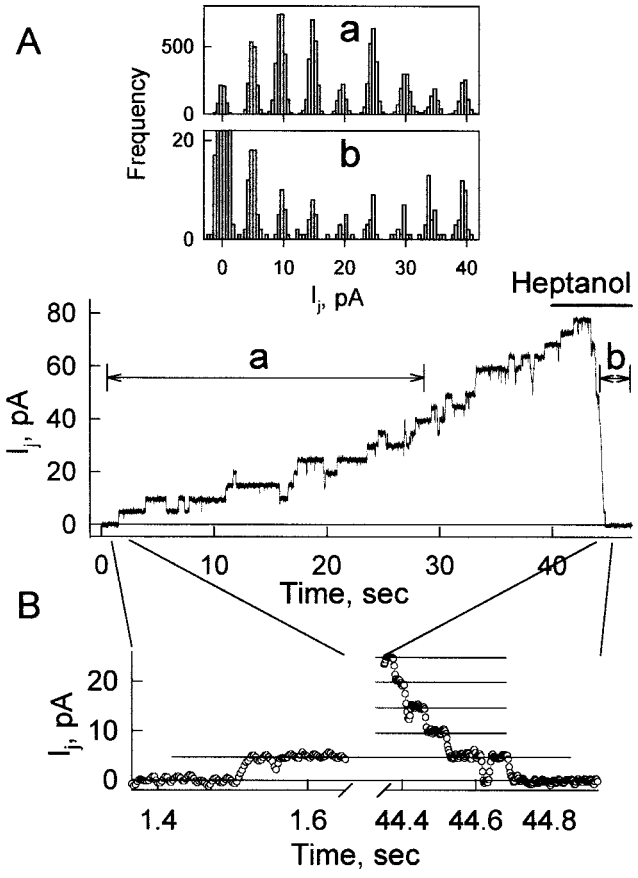

FIGURE 11 Illustration of Cx43-EGFP channel gating caused by heptanol. (*A*) Record of I_j showing recovery from a previous heptanol application and rapid uncoupling during a subsequent reapplication of heptanol. Individual channel transitions are evident on washout and reapplication. Junctional current histograms obtained from the indicated segments (*a* and *b*) show uniform transition sizes of ~110 pS. V_j was held constant at 45 mV. (*B*) Expanded view of the beginning and the end of the record shown in *A*. Circles represent values of I_j at 2.5-ms intervals.

types of transitions and a molecular distinction, namely, that transitions to γ_{res} are selectively lost by the attachment of EGFP to the CT domain. The latter provides evidence that the two types of gating transitions do, in fact, represent different mechanisms with distinct molecular loci. Thus, in homotypic Cx43-EGFP channels the transitions to γ_{closed} underlie all the conductance changes observed macroscopically. These junctions are characterized by a G_j-V_j relation that is less steep than for Cx43, lacks a G_{min} and shows considerably slower kinetics of decay and recovery of I_j. In correlating macroscopic and single-channel recordings of Cx43 junctions, we also observe that there can be slow kinetic changes in I_j and that they occur concomitant with the appearance of transitions to γ_{closed}. At small V_j values, the transitions to γ_{closed} are present and occur only from γ_{open}. At large V_j, exceeding ± 100, the transitions to γ_{closed} are more frequent, but occur almost exclusively from γ_{res} as the channels are first driven into γ_{res}. Correspondingly, macroscopic I_j shows rapid and slow components of decay and recovery and an increase in the slow component concomitant with an increase in the frequency of transitions to γ_{closed}. Surprisingly, at intermediate voltages, especially near ± 80 mV, transitions to γ_{closed} are nearly absent, as is a slow component to the decay and recovery of macroscopic I_j. In heterotypic Cx43/Cx43-EGFP junctions, these gating properties appear to segregate with the corresponding hemichannels.

Our data can be explained by having two gates in series in each hemichannel, as diagramed schematically in Fig. 12 *A*, with the state of one gate contingent on the state of the other. We refer to the gate mediating fast transitions to γ_{res} as the fast gate and the gate mediating to γ_{closed} as the slow gate. With both gates sensitive to V_j and not V_m (see Fig. 2), the sensors for these gates likely reside in or near the channel pore where they can sense the local field induced by V_j (Harris et al., 1981; Verselis et al., 1994). Homotypic Cx43-EGFP junctions lack the fast gate on both sides and the heterotypic Cx43/Cx43-EGFP junctions on one side (Fig. 12, *B* and *C*). The G_j-V_j relation of the slow gating mechanism alone, taken from cell pairs expressing Cx43-EGFP is shown in Fig. 12 *D* (solid line) along with the G_j-V_j relation expected for the fast V_j gating mechanism alone (dashed line). Because of its sensitivity to V_j, closure of the slow gate will dominate at small V_j values giving rise to a dominance of gating transitions from γ_{open} to γ_{closed}. With larger V_j values that invoke closure of the fast gate, faster kinetics of closure would tend to first close the fast gate resulting in a large fraction of the V_j gradient dropping across the region of the pore narrowed by its closure. Closure of the fast gate would reduce the V_j gradient at the sensor for the slow gate, which would tend to keep it open. At a sufficiently large V_j, the V_j gradient would be large enough to effect closure of the slow gate, even with the fast gate closed, giving rise to a reemergence of transitions to γ_{closed}, but from γ_{res} rather than from γ_{open}. The expected G_j-V_j relation for the fast V_j gating mechanism (see dashed line in Fig. 12 *D*) was derived from a Boltzmann relation with $V_0 = \pm 50$ mV, close to that measured in Cx43 channels, and $G_{min} = 0.25$, equal to the ratio $\gamma_{res}/\gamma_{open}$ we measured for Cx43. A value of 0.2 mV^{-1} was assigned to A, close to that obtained from G_j-V_j relations of Cx40 and Cx47 homotypic junctions; the latter exhibit G_{min} close to the ratios $\gamma_{res}/\gamma_{open}$ and fast g_j recovery, suggesting that the V_j sensitivity of the slow gating mechanism is shifted to larger V_j values (Bukauskas et al., 1995a; Teubner et al., 2001).

Using the large differences in the kinetics of recovery of the fast and slow V_j gating mechanisms, we measured the ratio g_{jpost}/g_{jpre}, which provided an estimate of the fraction of channels with slow gates closed. In Cx43-EGFP channels this ratio decreases monotonically with V_j (Fig. 6 *A*), following the G_j-V_j relationship as expected for channels containing only the slow gate. The V_j at which half the channels

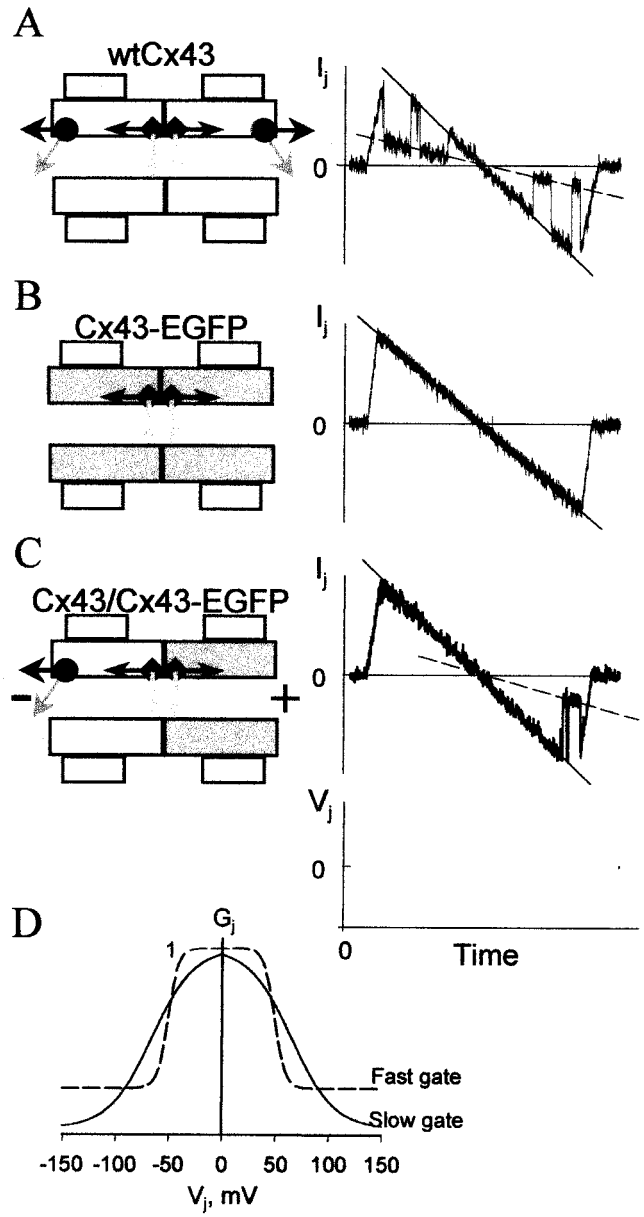

FIGURE 12 Schematic illustration of homo- and heterotypic GJ channels assembled from Cx43 and Cx43-EGFP and gating. To the right of each type of channel are examples of single-channel currents recorded in response to 2-s, ±100-mV V_j ramps. (*A*) A homotypic Cx43 channel contains fast and slow V_j gates represented by arrows with circles and diamonds, respectively. Each hemichannel possesses both gates. Closure of the fast gates, one per each V_j polarity, result in gating to the residual state. (*B*) A homotypic Cx43-EGFP channel contains only the slow V_j gate resulting in two series gates. Closure of the slow gate is rarely observed with 2-s ramps. (*C*) A heterotypic Cx43/Cx43-EGFP channel is asymmetric, possessing fast and slow gates in the Cx43 hemichannel and only the slow gate in the Cx43-EGFP hemichannel. This configuration results in three series gates. Closure of the fast gate to the residual state is observed only for V_j values relatively negative on the Cx43 side. (*D*) Illustration of the G_j-V_j relations of the fast (— — —) and slow (——) gating mechanisms. The G_j-V_j relation of the slow gating mechanism was obtained from Cx43-EGFP channels lacking the fast mechanism. The G_j-V_j relation of the fast gating mechanism is hypothetical and has the following Boltzmann parameters: $V_0 = 50$ mV, $A = 0.2$ mV^{-1}, and $G_{min} = 0.25$ (see Discussion).

closed on average is ~65 mV. In Cx43 channels, we found that this ratio has a maximum at V_j of ~80 mV, indicating that ~95% of channels are closed to the residual state when we observe channels to gate almost exclusively to γ_{res}. This ratio decreases at both at small and large V_j when full closures to γ_{closed} are observed (see Figs. 6 and 8 *C*). At a large V_j of ~150 mV the ratio is ~0.5, or half the channels fully closed, similar to that which is obtained at 65 mV for channels lacking the fast gate. This would suggest that when fast gate is closed to γ_{res} the slow gate senses only ~40% of the voltage drop compared with when channel is open. However, we cannot exclude that conformational changes leading to the channel closure to γ_{res} affect the shape of the G_j-V_j relation of the slow gating mechanism, e.g., by a change in orientation or position of the sensor, etc.

Locations of fast and slow gates

That fast V_j gating to γ_{res} is a property of hemichannels has been established in studies of cell-cell channels and unapposed hemichannels (Verselis et al., 1994; Bukauskas and Weingart, 1994; Bukauskas et al., 1995a,b; Trexler et al., 1996; Oh et al., 2000). Molecular studies of Cx32 and Cx26 indicate that the NT comprises an integral component of a hemichannel's V_j sensor for the fast gate (Verselis et al., 1994; Oh et al., 2000). The NT domain is on the cytoplasmic side, and loss of V_j gating to γ_{res} by the attachment of EGFP to the CT of Cx43, which is also on the cytoplasmic side, suggests that there may be interactions among cytoplasmic domains that are important for fast V_j gating. Similarly, attachment of aequorin to the CT of Cx32 or Cx43 was shown to slow down the time course of decrease in g_j with V_j (Martin et al., 1998), as did truncation of the CT domains of these connexins (Revilla et al., 1999). Peracchia et al. (1999) also demonstrated that mutations in the CT domain of Cx32, as well as the creation of a tandem protein linking the CT of one Cx32 molecule to the NT of another, dramatically affected V_j-sensitive gating. All of these data indicate that the structure that mediates fast V_j gating in Cx43, and perhaps Cx32, includes areas of the CT and NT domains. Loss of fast V_j gating without an effect on open-channel conductance, permeability to fluorescent dyes, and susceptibility to chemical uncouplers, suggests that the attachment of EGFP to CT does not cause gross changes in channel structure but immobilizes the fast V_j gate in the open state either by steric interference or by disruption of the transduction mechanism that links movement of the V_j sensor to channel closure. Mutation of a proline residue in TM2 was shown to strongly affect V_j gating (Suchyna et al., 1993) and to behave in a manner consistent with a proline kink motif (Ri et al., 1999). The conformational changes mediated by the proline kink motif in TM2 are proposed to narrow the cytoplasmic end of the channel supporting a cytoplasmic location for the V_j gate.

Given that unapposed hemichannels show both types of gating, slow gates are also likely a property of the hemichannel (Trexler et al., 1996; Oh et al., 2000). Slow gating in hemichannels was provisionally ascribed to the extracellular loops because it resembled the gating shown by Bukauskas and Weingart (1994), to be associated with initial opening during cell-cell channel formation, and showed strong sensitivity to extracellular Ca^{2+} (Trexler et al., 1996). The substituted cysteine accessibility method applied to Cx46 hemichannels reported loss of accessibility of the L35 residue in TM1 upon closure of the slow gate, indicating a location of the slow gate extracellular to this position (Pfahnl and Dahl, 1998). Thus, in unapposed hemichannels, we provisionally place the slow gate extracellular to the fast gate. However, the slow gate has not been selectively abolished or modified and shown to be correspondingly altered for only one polarity of V_j in a cell-cell channel. Thus, it is possible that the slow gate constitutes a single gate in cell-cell channels formed by the interacting extracellular loop domains. We view this possibility less likely as it would require a single gate to close for both polarities of V_j.

Gating polarities and fast and slow gates

Published data regarding the gating polarity of the fast V_j gate of Cx43 are controversial. Based on asymmetry of V_j gating in heterotypic junctions formed between *Xenopus* oocytes expressing Cx43 and those expressing the endogenous *Xen*Cx38, Cx43 hemichannels appeared to close on relative positivity on their cytoplasmic side (Swenson et al., 1989; Werner et al., 1989). In other studies using mammalian cell lines (Moreno et al., 1995) as well as *Xenopus* oocytes (Steiner and Ebihara, 1996), heterotypic junctions formed between cells expressing Cx43 and those expressing Cx45 suggested that Cx43 and Cx45 hemichannels closed on relative negativity on their cytoplasmic sides. These apparent discrepancies suggest that the gating properties of hemichannels can depend to varying degrees on the type of hemichannel with which they are paired. In many cases, the changes are small in that the gating behavior is very close to that of hemichannels seen in other pairing combinations, although the g_j-V_j relation may be altered in steepness or shifted along the V_j axis. For Cx43, the effects appear to be more dramatic, with Cx43 in *Xen*Cx38/Cx43 junctions appearing to have the opposite V_j gating polarity from that of Cx43 in Cx43/Cx45 junctions. Results of this kind led to the suggestion that V_j gating is not an intrinsic property of the hemichannel (White et al., 1994) but was based on the assumption that a single voltage-gating mechanism is present in GJ channels. The existence of two types of V_j-sensitive gates, with each type potentially modulated by hemichannel interactions, can create a variety of g_j-V_j relations in heterotypic junctions that could deviate from the simple asymmetries predicted from the corresponding homotypic junctions. We suggest that Cx43/Cx43-EGFP channels can be viewed as pseudo-homotypic channels because the sequences of the two hemichannels in extracellular and transmembrane regions are identical. The intrinsic gating properties of Cx43 hemichannels are likely to be affected in the same way by hemichannel interactions both in homotypic Cx43 channels and in heterotypic Cx43/Cx43-EGFP channels. From this assumption and the gating asymmetry of Cx43/Cx43-EGFP channels (Figs. 8 and 9), we conclude that in Cx43 channels the fast gate closes in the hemichannel that is made relatively negative on its cytoplasmic side. This is shown in the schematic illustration of a heterotypic gap junction channel, demonstrating asymmetric V_j gating with fast I_j transitions between open and residual states at negativity from the Cx43 hemichannel side (Fig. 12 *C*). Because both hemichannels retain the slow gate, we cannot definitively assign its gating polarity.

Chemical gating of Cx43-EGFP channels

Attachment of EGFP to the CT of Cx43 selectively disrupts fast V_j gating to γ_{res} but preserves both slow V_j gating and gating by chemical agents. Closure of channels by chemical agents, particularly fatty acids and alkanols, has been suggested to occur by perturbation of the channel at the lipid-channel interface (Burt et al., 1991). Previously we showed that clusters or plaques of GJ channels can be resolved in living cells at locations of cell-cell contact using Cx43-EGFP and that plaques are required for electrical coupling (Bukauskas et al., 2000). Here we monitored fluorescence of plaques in electrically coupled cell pairs and showed that exposure to the uncoupling agent heptanol caused complete uncoupling but no measurable change in fluorescence intensity or size and shape of the plaque. Thus, the uncoupling effect of alkanols is not related to dispersion of junctional plaques. Similarly, plaques did not show evidence of dispersing when exposed to CO_2. However, fluorescence of GFP and other color variants are known to be sensitive to pH (reviewed by Tsien, 1998), and by lowering cytoplasmic pH with CO_2 we observed that EGFP retained its pH sensitivity when attached to Cx43 (Fig. 10 *C*). Thus, connexins fused to EGFP, or more appropriately with mutants of GFP selected for their pH-sensitive properties (Miesenbock et al., 1998), can be exploited to measure intracellular pH in very close proximity to the junctions and better quantitate conductance changes with pH.

In summary, Cx43 GJ channels contain two types of gate sensitive to V_j: one characterized by fast gating transitions to the residual state and the other by slow gating transitions to the fully closed state. These two mechanisms interact in a manner consistent with contingent gating and placement of the gating elements in series in the pore. Fast V_j gating is selectively lost in Cx43-EGFP channels and this loss is confined to the hemichannel composed of Cx43-EGFP. Gating asymmetry in Cx43/Cx43-EGFP heterotypic chan-

nels shows that the fast V_j gate has a negative gating polarity; i.e., the hemichannel closes when its cytoplasmic face is made relatively negative. We suggest that all connexins that form GJ channels contain two V_j gates and that relative differences in sensitivity and kinetics of V_j dependence of these gates provide the complex array of gating properties observed among GJ channels. Indeed, both types of gating transitions have been reported in channels formed of Cx26, Cx32, Cx37, and Cx40 (Bukauskas et al., 1995a,b; Oh et al., 1999; Ramanan et al., 1999). All GJ channels also display chemical gating, and this form of gating shares several features in common with slow V_j gating. Both mechanisms close channels completely, and closures are characterized by slow transitions to a fully closed state (Bukauskas and Peracchia, 1997). Also, chemically induced uncoupling by alkanols, Ca^{2+}, and H^+ was shown to be reversible by voltage (Obaid et al., 1983; Weingart and Bukauskas, 1998; Peracchia et al., 1999). Taken together, these data support the possibility that chemical gating and slow V_j gating share common structural elements.

We thank Dr. Laird for kindly providing us with the Cx43-EGFP construct and Dr. Klaus Willecke and Dr. Ross Johnson for kindly providing us with the HeLaCx43 and Novikoff cell lines. We thank Dr. Seunghoon Oh and Dr. Brady Trexler for valuable technical help.

This study was supported by National Institutes of Health grants NS36706 to F.F.B. and GM54179 to V.K.V.

REFERENCES

Banach, K., and R. Weingart. 2000. Voltage gating of Cx43 gap junction channels involves fast and slow current transitions. *Pflugers Arch.* 439:248–250.

Barrio, L. C., J. Capel, J. A. Jarillo, C. Castro, and A. Revilla. 1997. Species-specific voltage-gating properties of connexin-45 junctions expressed in *Xenopus* oocytes. *Biophys. J.* 73:757–769.

Bennett, M. V., and V. K. Verselis. 1992. Biophysics of gap junctions. *Semin. Cell Biol.* 3:29–47.

Bukauskas, F. F., C. Elfgang, K. Willecke, and R. Weingart. 1995a. Biophysical properties of gap junction channels formed by mouse connexin40 in induced pairs of transfected human HeLa cells. *Biophys. J.* 68:2289–2298.

Bukauskas, F., C. Elfgang, K. Willecke, and R. Weingart. 1995b. Heterotypic gap junction channels (connexin26–connexin32) violate the paradigm of unitary conductance. *Pflugers Arch.* 429:870–872.

Bukauskas, F. F., K. Jordan, A. Bukauskiene, M. V. Bennett, P. D. Lampe, D. W. Laird, and V. K. Verselis. 2000. Clustering of connexin 43-enhanced green fluorescent protein gap junction channels and functional coupling in living cells. *Proc. Natl. Acad. Sci. U.S.A.* 97:2556–2561.

Bukauskas, F., C. Kempf, and R. Weingart. 1992. Electrical coupling between cells of the insect *Aedes albopictus*. *J. Physiol.* 448:321–337.

Bukauskas, F. F., and C. Peracchia. 1997. Two distinct gating mechanisms in gap junction channels: CO_2-sensitive and voltage-sensitive. *Biophys. J.* 72:2137–2142.

Bukauskas, F. F., and R. Weingart. 1994. Voltage-dependent gating of single gap junction channels in an insect cell line. *Biophys. J.* 67: 613–625.

Burt, J. M., K. D. Massey, and B. N. Minnich. 1991. Uncoupling of cardiac cells by fatty acids: structure-activity relationships. *Am. J. Physiol.* 260:C439–C448.

Ebihara, L., and E. Steiner. 1993. Properties of a nonjunctional current expressed from a rat connexin46 cDNA in *Xenopus* oocytes. *J. Gen. Physiol.* 102:59–74.

Harris, A. L., D. C. Spray, and M. V. Bennett. 1981. Kinetic properties of a voltage-dependent junctional conductance. *J. Gen. Physiol.* 77: 95–117.

Jordan, K., J. L. Solan, M. Dominguez, M. Sia, A. Hand, P. D. Lampe, and D. W. Laird. 1999. Trafficking, assembly, and function of a connexin43-green fluorescent protein chimera in live mammalian cells. *Mol. Biol. Cell.* 10:2033–2050.

Manthey, D., F. Bukauskas, C. G. Lee, C. A. Kozak, and K. Willecke. 1999. Molecular cloning and functional expression of the mouse gap junction gene connexin-57 in human HeLa cells. *J. Biol. Chem.* 274: 14716–14723.

Martin, P. E., C. H. George, C. Castro, J. M. Kendall, J. Capel, A. K. Campbell, A. Revilla, L. C. Barrio, and W. H. Evans. 1998. Assembly of chimeric connexin-aequorin proteins into functional gap junction channels. Reporting intracellular and plasma membrane calcium environments. *J. Biol. Chem.* 273:1719–1726.

Meyer, R. A., P. D. Lampe, B. Malewicz, W. J. Baumann, and R. G. Johnson. 1991. Enhanced gap junction formation with LDL and apolipoprotein B. *Exp. Cell Res.* 196:72–81.

Miesenbock, G., D. A. De Angelis, and J. E. Rothman. 1998. Visualizing secretion and synaptic transmission with pH-sensitive green fluorescent proteins. *Nature.* 394:192–195.

Moreno, A. P., E. C. Beyer, B. I. Fishman, and D. C. Spray. 1995. Voltage dependent gating and single channel analysis of heterotypic gap junction channels formed of Cx45 and Cx43. *Prog. Cell Res.* 4:405–408.

Moreno, A. P., M. B. Rook, G. I. Fishman, and D. C. Spray. 1994. Gap junction channels: distinct voltage-sensitive and -insensitive conductance states. *Biophys. J.* 67:113–119.

Neyton, J., and A. Trautmann. 1985. Single-channel currents of an intercellular junction. *Nature.* 317:331–335.

Obaid, A. L., S. J. Socolar, and B. Rose. 1983. Cell-to-cell channels with two independent regulated gates in series: analysis of junctional channel modulation by membrane potential, calcium and pH. *J. Membr. Biol.* 73:69–89.

Oh, S., C. K. Abrams, V. K. Verselis, and T. A. Bargiello. 2000. Stoichiometry of transjunctional voltage-gating polarity reversal by a negative charge substitution in the amino terminus of a connexin32 chimera. *J. Gen. Physiol.* 116:13–32.

Oh, S., J. B. Rubin, M. V. Bennett, V. K. Verselis, and T. A. Bargiello. 1999. Molecular determinants of electrical rectification of single channel conductance in gap junctions formed by connexins 26 and 32. *J. Gen. Physiol.* 114:339–364.

Peracchia, C., X. G. Wang, and L. L. Peracchia. 1999. Is the chemical gate of connexins voltage sensitive? Behavior of Cx32 wild-type and mutant channels. *Am. J. Physiol.* 276:C1361–C1373.

Perez-Armendariz, E. M., M. C. Romano, J. Luna, C. Miranda, M. V. Bennett, and A. P. Moreno. 1994. Characterization of gap junctions between pairs of Leydig cells from mouse testis. *Am. J. Physiol.* 267: C570–C580.

Pfahnl, A., and G. Dahl. 1998. Localization of a voltage gate in connexin46 gap junction hemichannels. *Biophys. J.* 75:2323–2331.

Pfahnl, A., and G. Dahl. 1999. Gating of cx46 gap junction hemichannels by calcium and voltage. *Pflugers Arch.* 437:345–353.

Ramanan, S. V., P. R. Brink, K. Varadaraj, E. Peterson, K. Schirrmacher, and K. Banach. 1999. A three-state model for connexin37 gating kinetics. *Biophys. J.* 76:2520–2529.

Revilla, A., M. V. Bennett, and L. C. Barrio. 2000. Molecular determinants of membrane potential dependence in vertebrate gap junction channels. *Proc. Natl. Acad. Sci. U.S.A.* 97:14760–14765.

Revilla, A., C. Castro, and L. C. Barrio. 1999. Molecular dissection of transjunctional voltage dependence in the connexin-32 and connexin-43 junctions. *Biophys. J.* 77:1374–1383.

Ri, Y., J. A. Ballesteros, C. K. Abrams, S. Oh, V. K. Verselis, H. Weinstein, and T. A. Bargiello. 1999. The role of a conserved proline

residue in mediating conformational changes associated with voltage gating of Cx32 gap junctions. *Biophys. J.* 76:2887–2898.

Steiner, E., and L. Ebihara. 1996. Functional characterization of canine connexin45. *J. Membr. Biol.* 150:153–161.

Suchyna, T. M., L. X. Xu, F. Gao, C. R. Fourtner, and B. J. Nicholson. 1993. Identification of a proline residue as a transduction element involved in voltage gating of gap junctions. *Nature.* 365:847–849.

Swenson, K. I., J. R. Jordan, E. C. Beyer, and D. L. Paul. 1989. Formation of gap junctions by expression of connexins in *Xenopus* oocyte pairs. *Cell.* 57:145–155.

Teubner, B., B. Odermatt, M. Güldenagel, G. Söhl, J. Degen, F. Bukauskas, J. Kronengold, V. K. Verselis, Y. Jung, C. Kozak, K. Schilling, and K. Willecke. 2001. Functional expression of the new gap junction gene connexin47 transcribed in mouse brain and spinal cord neurons. *J. Neurosci.* 21:1117–1126.

Trexler, E. B., M. V. Bennett, T. A. Bargiello, and V. K. Verselis. 1996. Voltage gating and permeation in a gap junction hemichannel. *Proc. Natl. Acad. Sci. U.S.A.* 93:5836–5841.

Tsien, R. Y. 1998. The green fluorescent protein. *Annu. Rev. Biochem.* 67:509–544.

Valiunas, V., F. F. Bukauskas, and R. Weingart. 1997. Conductances and selective permeability of connexin43 gap junction channels examined in neonatal rat heart cells. *Circ. Res.* 80:708–719.

Verselis, V. K., M. V. Bennett, and T. A. Bargiello. 1991. A voltage-dependent gap junction in *Drosophila melanogaster*. *Biophys. J.* 59: 114–126.

Verselis, V. K., C. S. Ginter, and T. A. Bargiello. 1994. Opposite voltage gating polarities of two closely related connexins. *Nature.* 368:348–351.

Verselis, V. K., and R. Veenstra. 2000. Gap junction channels. Permeability and voltage gating. *Adv. Mol. Cell Biol.* 30:129–192.

Weingart, R., and F. F. Bukauskas. 1993. Gap junction channels of insects exhibit a residual conductance. *Pflugers Arch.* 424:192–194.

Weingart, R., and F. F. Bukauskas. 1998. Long-chain *n*-alkanols and arachidonic acid interfere with the Vm-sensitive gating mechanism of gap junction channels. *Pflugers Arch.* 435:310–319.

Werner, R., E. Levine, C. Rabadan Diehl, and G. Dahl. 1989. Formation of hybrid cell-cell channels. *Proc. Natl. Acad. Sci. U.S.A.* 86:5380–5384.

Wilders, R., and H. J. Jongsma. 1992. Limitations of the dual voltage clamp method in assaying conductance and kinetics of gap junction channels. *Biophys. J.* 63:942–953.

White, T. W., R. Bruzzone, D. A. Goodenough, and D. L. Paul. 1994. Voltage gating of connexins. *Nature.* 371:208–209.

White, R. L., D. C. Spray, C. A. C. Campos de, B. A. Wittenberg, and M. V. Bennett. 1985. Some electrical and pharmacological properties of gap junctions between adult ventricular myocytes. *Am. J. Physiol.* 249: C447–C455.